Doping of a surface band on Si(111)$\sqrt{3}\times\sqrt{3}$-Ag

J. N. Crain,[1] M. C. Gallagher,[2] J. L. McChesney,[1] M. Bissen,[3] and F. J. Himpsel[1]
[1]*Department of Physics, UW-Madison, 1150 University Avenue, Madison, Wisconsin 53706, USA*
[2]*Department of Physics, Lakehead University, Thunder Bay, Ontaria, Canada P7B 5E1*
[3]*Synchrotron Radiation Center, UW-Madison, 3731 Schneider Drive, Stoughton, Wisconsin 53589, USA*
(Received 6 January 2005; published 7 July 2005)

A semiconducting surface-state band on Si(111)$\sqrt{3}\times\sqrt{3}$-Ag is doped by adsorption of additional Ag and Au atoms. Very high levels of doping can be achieved (0.0015–0.086 electrons per 1×1 unit cell), such that the silicon surface degenerates into a metal. The doping alters the band structure of the surface state and causes the rigid-band model to break down. The parabolic-band approximation breaks down as well. These observations shed light on the mechanism of doping at extreme levels.

DOI: 10.1103/PhysRevB.72.045312 PACS number(s): 73.20.At, 79.60.Jv, 73.25.+i

The mechanism of doping becomes nontrivial at extreme carrier densities. Modeling a dopant by an isolated perturbation of the lattice with its own localized wave function fails as the wave functions of adjacent dopants begin to overlap and to form their own band. Eventually, a semiconductor degenerates into a metal. This transition has been studied in the bulk. Here we address its two-dimensional version, where a semiconductor surface is converted into a two-dimensional metal by doping a surface-state band. This phenomenon may be viewed as a surface analog of the two-dimensional electron gas at semiconductor interfaces, which has been used extensively for studying new phases of electrons and producing high-speed electronic devices. With surface doping one is able to reach much higher doping levels than at interfaces, which makes it possible to explore the breakdown of low-density approximations and observe the degenerate, metallic version of the two-dimensional electron gas.

Metallization of semiconductor surfaces has been observed in several cases, and several mechanisms have been used to explain it. The Fermi level at the surface of InAs and InSb is pinned inside the bulk conduction band, which causes a charge transfer from the bulk to the surface and the formation of a two-dimensional electron gas.[1,2] Another type of bulk-to-surface charge transfer has been observed on the Si(111)2×1 and Si(100)2×1 surfaces,[3–5] where n-type bulk dopants transfer their charge to empty π^* surface bands. A third type of surface metallization has been observed for the Si(111)$\sqrt{3}\times\sqrt{3}$-Ag structure and related superlattices.[6–19] In that case, the surface is semiconducting for a stoichiometric surface with exactly one Ag atom per 1×1 unit cell,[16] and adsorption of additional Ag or Au atoms dopes a semiconducting surface band with electrons.[9] Recent studies of one-dimensional structures induced by Au on vicinal Si(111) surfaces indicate that this type of doping mechanism plays a key role in stabilizing one-dimensional structures by enabling the optimal band filling.[20–22] The Fermi surface is automatically nested in one dimension and thus provides a much stronger electronic driving force for charge-density waves and surface reconstructions than in higher dimensions.

We use angle-resolved photoemission to observe the doping-induced evolution of the semiconducting surface-state band on Si(111)$\sqrt{3}\times\sqrt{3}$-Ag. Addition of Ag to the full monolayer of the $\sqrt{3}\times\sqrt{3}$ structure allows us to convert the semiconducting surface to a metal in a controlled way and to map out the changes in the $E(k)$ band dispersion and the Fermi surface. A breakdown of the rigid-band model occurs at high doping levels. The bottom of the surface band moves from 0.19 eV above the bulk valence-band maximum (VBM) to 0.30 eV below the VBM for high doping. A further departure from the simple bulk doping model is the nonparabolic behavior that is observed for higher dopings. Kinks in the band dispersion that are accompanied by dips in the photoemission intensity suggest interaction with an impurity state. A first-principles calculation[23] for one-third of a monolayer of extra Ag atoms on $\sqrt{3}\times\sqrt{3}$-Ag provides a plausible explanation for both the downward shift in E_0 with increasing coverage and the impurity state near E_F.

Precise electron doping levels ranging from 0.0015 to 0.086 electrons per 1×1 cell are achieved in a two-step process. First, slightly more than one monolayer Ag is deposited and excess Ag is driven off by annealing for a few seconds at $\sim$600 °C (see Refs. 16 and 18). Low-energy electron diffraction LEED showed a clear $\sqrt{3}\times\sqrt{3}$ pattern with no evidence of 6×1 domains that form near step edges for longer anneals.[18] Subsequently, low doping levels are achieved by depositing excess Ag onto the stoichiometric surface and annealing at low temperatures below 200 °C. The area inside the Fermi surfaces in Fig. 1 is used as a measure of the doping using Luttinger's theorem, which holds as long the electron-electron interactions can be described by perturbation theory.[24] The ratio between the area inside the Fermi surface and the unit cell in reciprocal space, with a factor of two electrons per filled band, gives the number of electrons per unit cell in real space. Since the $\sqrt{3}\times\sqrt{3}$ unit cell is three times larger than the 1×1 unit cell in real space, we divide by an additional factor of 3 to find the numbers of electrons per Si(111) 1×1 cell, as reported in Fig. 1.

The photoemission data were acquired with a Scienta 200 spectrometer with E,ϑ multidetection and an energy resolution of 20 meV for electrons and 7 meV for photons (see Ref. 17 for details on the acquisition of Fermi surfaces). We used p-polarized synchrotron radiation at a photon energy $h\nu=34$ eV, where the cross section of silicon surface states

 ©2005 The American Physical Society

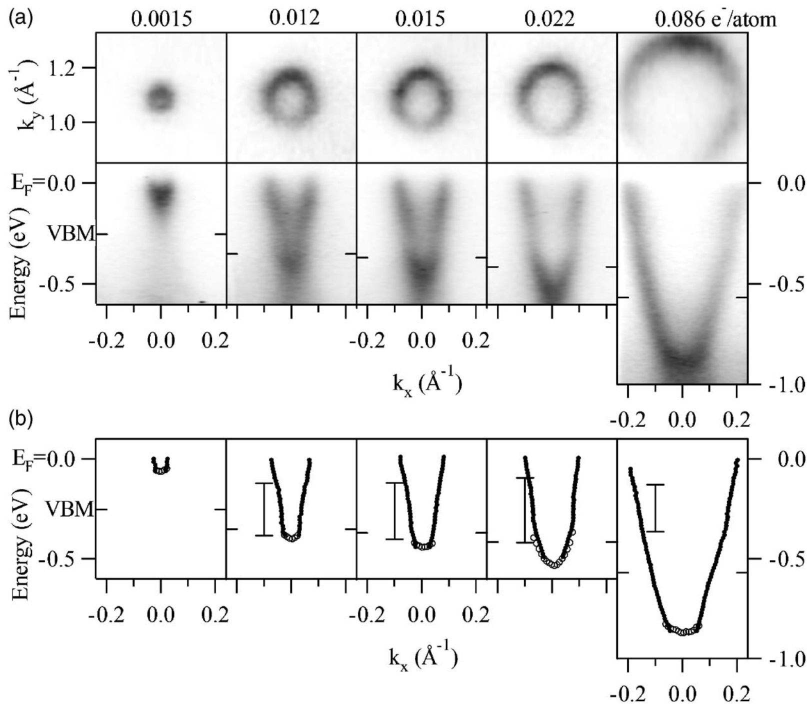

FIG. 1. (a) Fermi surfaces (top) and band dispersions (bottom) for $Si(111)\sqrt{3}\times\sqrt{3}-Ag$ surfaces doped by various amounts of excess Ag [0.0015, 0.012, 0.015, 0.022, and 0.086 extra electrons per Si(111) 1×1 unit cell]. High photoemission intensity is shown dark. k_x is along $[\bar{1}\,\bar{1}2]$, k_y is along $[\bar{1}10]$, and the centers of the Fermi circles (top) are at the $\bar{K}$ point of the 1×1 Brillouin zone. (b) Band dispersions extracted from (a) by fitting MDCs (full circles) and EDCs (open circles). The vertical bars delineate a dip in the intensity due to interaction with a second band (see Figs. 3 and 4). The energy is relative to the Fermi level E_F with the valence-band maximum indicated by horizontal tickmarks.

has a maximum relative to the bulk states.[25,26] Figure 1 gives an overview of the Fermi surfaces and band dispersions $E(k_x)$ along the the $[\bar{1}\,\bar{1}2]$ direction for various levels of Ag doping. These are used to determine the doping dependence of the band energies plotted in Fig. 2. Figures 3 and 4 show band dispersions for specific doping with Ag and Au, respectively. The photoemission intensity is plotted on a gray scale with high intensity shown dark.

The measurements are performed at low temperatures (<60 K) in order to reduce phonon broadening and to provide a sharper Fermi level cutoff. The increased carrier lifetime causes a substantial photovoltage to build up for high-quality surfaces [−0.82 eV for n-type and +0.06 eV for p-type samples of $Si(111)\sqrt{3}\times\sqrt{3}$-Ag at low doping]. The Fermi cutoff allows us to obtain the position of the valence-band maximum relative to E_F, which is indicated by tickmarks in Fig. 1. The photovoltage is measured at E_F and subtracted directly from the Si $2p$ core level. To keep the sample potential well defined we saturate the photovoltage by illumination with an extra spotlight during measurements. Thereby, residual variations in the sample potential with angle, synchrotron light intensity, and photon energy are minimized. As a consistency check, the absolute value of the photovoltage provides a lower bound for the Schottky barrier (E_F minus VBM for p type, CBM minus E_F for n type where CBM is the conduction-band minimum). This con-

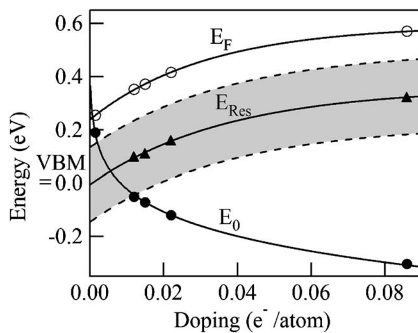

FIG. 2. The Fermi energy E_F, the band minimum E_0, and the resonance energy E_{res} as a function of doping [in electrons per Si(111) 1×1 cell]. All energies are plotted with respect to the valence-band maximum (VBM). For our range of doping the surface band moves from 0.19 eV above the VBM to 0.30 eV below the VBM, which demonstrates a breakdown of the rigid-band model. The resonance energy tracks the Fermi level at a constant offset of −0.25 eV. Below 0.007 doping it dips below the conduction-band minimum of the surface state and behaves like a donor level.

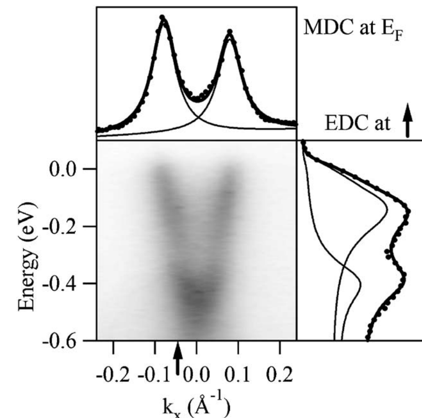

FIG. 3. Full band dispersion (gray-scale image) for $Si(111)\sqrt{3}\times\sqrt{3}$-Ag doped by 0.015 electrons per 1×1 unit cell combined with MDCs (horizontal cuts) and EDCs (vertical cuts). MDCs provide a symmetric Lorentzian line shape and produce sharp peaks for steep band sections. EDCs produce sharp peaks for flatband sections, such as the bottom of the band, and reveal the intensity drop due to interaction with an impurity state.

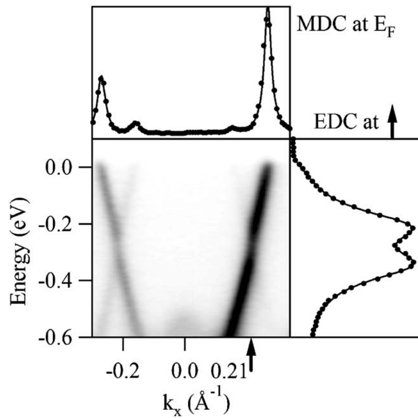

FIG. 4. Similar to Fig. 3 but for a $\sqrt{21}\times\sqrt{21}$ superlattice formed by 0.2 monolayers of Au doping Si(111)$\sqrt{3}\times\sqrt{3}$-Ag. Avoided crossings between superlattice bands lead to dips in the intensity similar to that in Fig. 3.

strains the possible range of the Fermi level in the gap of bulk Si yielding $E_F - E_{\mathrm{VBM}} = 0.17 \pm 0.11$ eV for Si(111)$\sqrt{3}\times\sqrt{3}$-Ag at low doping.

A breakdown of the rigid-band model can be detected right away in Figs. 1 and 2 by observing the change of the bottom of the band, E_0, relative to the VBM when the doping is increased. In a simple rigid-band model the surface bands are tied to the bulk bands, and doping with electrons just pushes the Fermi level higher up relative to the VBM. Plotting E_0 and E_F relative to the VBM in Fig. 2 versus doping quantifies the deviations from the rigid-band model. From the change in E_0 with doping, we conclude that the rigid-band model fails over the entire range of coverages studied, from 1.2×10^{12} to 6.7×10^{14} electrons/cm^2. Even the lowest doping level, which is well below values reported in previous studies,[19] is within the moderate- to high-doping regime when compared to similar dopant spacings for bulk silicon (a comparable spacing would give a density of 1×10^{18} electrons/cm^3). At extremely small doping levels we still expect the rigid-band model to hold, but this will require systematic experiments at even lower doping levels. Such experiments will push the limits of current sample quality and detector resolution. Close to zero doping we would expect a donor level to move above E_F, as indicated by the extrapolation of the data towards zero doping in Fig. 2.

A second feature of the surface band that goes beyond simple models of doping is the deviation from parabolicity. Instead of parabolas, we find kinked bands with slopes that appear to become shallower as they approach the Fermi level. We attribute these perturbations to a crossing with a defect state associated with the Ag impurities. The nonparabolicity we observe might explain some of the variations of the effective masses reported in the literature.[11,17,19] Furthermore, as part of the breakdown of the rigid-band model we find that the Fermi velocity and effective mass change continuously with doping level, which makes comparison of different studies with different dopings difficult. As the doping increases and the bottom of the surface state crosses the valence-band maximum, the effective mass increases. Even in previous studies at lower dopings,[17,19] where the bands appear to be still parabolic, this doping dependence must be considered in comparing the effective masses.

A recent combined photoemission and scanning tunneling spectroscopy study pointed out a technical difficulty: determining band dispersions from either separate energy distribution curves (EDCs) or momentum distribution curves (MDCs) can be prone to systematic errors in the fitting.[19] Further, they propose a method for directly fitting the two-dimensional dispersion with a parabola. However, such a method is impractical for band dispersions that are clearly nonparabolic like those in the present study. Instead, we take advantage of the best aspects of the two fitting methods. Momentum distribution curves, which provide sharp, symmetric peaks with a Lorentzian line shape (see Figs. 3 and 4), are used for steep sections of the band and EDCs are used for the flat region at the bottom where the MDCs become broad [full and open circles in Fig. 1(b)]. Both methods can be checked against each other in the overlap regions. MDCs are particularly useful for determining the Fermi surface (Figs. 3 and 4 top), as evident in Ref. 19, which obtains the same Fermi crossings using MDCs and a parabolic fit. EDCs provide the bottom of the band E_0 and further reveal a peculiar drop in the intensity (Fig. 3 right) that will be discussed next.

In addition to its nonparabolic shape, the surface band exhibits a drop in intensity at a particular energy. The evidence for this dip can be seen in the gray-scale band dispersions in Fig. 1(a) for the three intermediate doping levels, as well as in Fig. 3 (lower left and right). The anomalous energy region can be pinpointed by the double hump in the EDCs and small kinks in the band dispersion in Fig. 3. This resonance energy region is indicated by a vertical bar in Fig. 1(b) and has a center denoted as E_{res}. When plotted with respect to the VBM in Fig. 2 it is easy to see that E_{res} tracks the Fermi level, i.e., it is at a constant -0.25 ± 0.01 eV below E_F for all doping levels.

A natural explanation for the observed intensity dip would be an interaction of the surface state with an impurity state formed by the Ag dopants. At small doping the energy of the impurity state E_{res} starts out below the conduction-band minimum of the surface state (E_0) in Fig. 2. That is characteristic of a donor level for the two-dimensional surface state. At a doping of 0.007 e^-/atom the state E_{res} crosses E_0 and moves into the surface conduction band. Consequently, the impurity state hybridizes with the conduction-band continuum and forms a Fano resonance similar to the resonances observed between discrete excitations and a continuum in noble gases. The intensity minimum at E_{res} corresponds to destructive interference between the discrete state and the continuum, analogous to the $3s$-to-np transitions in Ar interacting with the $3p$ continuum at about 27 eV photon energy.[27] An impurity state caused by only a few percent of an electron per Si atom is easily missed in photoemission. Only its interference with the surface conduction band makes it visible at their crossing point in k space.

A first-principles calculation[23] for one-third of a monolayer of extra Ag atoms on $\sqrt{3}\times\sqrt{3}$-Ag shows just such an impurity state near E_F that is localized to the Ag impurities and has very flatband dispersion. A second highly dispersive band in the model corresponds well with the metallic

surface-state band that is filled by electrons from the extra Ag dopants. Thus, the first-principles model provides a plausible explanation both for the downward shift in E_0 with increasing coverage and for an impurity band near E_F.

The model of an impurity state crossing the surface state is also supported by an analogy to data from a related system where two superlattice bands form an avoided crossing (see Fig. 4). Similarly to Fig. 3, there is a dip in the EDC where the two bands meet. In that case the drop in intensity has been identified with a minigap that is associated with an avoided crossing of two bands with the same symmetry.[17] The two bands in Fig. 4 are both due to the $\sqrt{3}\times\sqrt{3}$-Ag surface band, folded back onto each other by the $\sqrt{21}\times\sqrt{21}$ superlattice formed by additional Au dopants. In Fig. 3 we suggest a similar interaction between the $\sqrt{3}\times\sqrt{3}$-Ag surface band and an impurity band formed by Ag dopants.

In addition to the impurity band model, one might consider an alternative explanation for the observed intensity dip due to the creation of defects during high-temperature annealing at 600 °C. Such annealing has been shown to produce narrow 3×1 domains along step edges, which have a lower density of Ag compared to the $\sqrt{3}\times\sqrt{3}$.[18] Even though we observe no sign of 3×1 domains in LEED, there is always the possibility of small 3×1 regions below our detection limit. Interactions with such 3×1 domains, or with Ag vacancies that form in neighboring $\sqrt{3}\times\sqrt{3}$ terraces, might also lead to the observed intensity dip.

In summary, we observe several departures from the conventional model of doping when the dopant density becomes so large that the dopants interact with each other and with the conduction band. This is demonstrated for a two-dimensional surface-state band on silicon that is doped by additional noble metal atoms. A detailed study of the band dispersion reveals a movement of the conduction band with doping that represents a departure from the rigid-band model. The bottom of the conduction band is nonparabolic, which indicates a breakdown of the effective mass approximation. Furthermore, a gap is observed in the conduction band that might be an indication of an interaction with an impurity state at high dopant concentration. Such specific experimental signatures should facilitate developing a quantitative, microscopic theory of the transition from a doped semiconductor to a metal. These concepts might be extendable to materials other than semiconductors, for example, the transition from magnetic impurity levels to an alloy band structure.[26,28]

We acknowledge experimental help from Ch. Gundelach, S. Janowski, and M. Fisher. The work was supported by the NSF under Award No. DMR-0240937. It was conducted in part at the Synchrotron Radiation Center, which is supported by the NSF under Award No. DMR-0084402.

[1] V. Y. Aristov, G. Le Lay, L. T. Vinh, K. Hricovini, and J. E. Bonnet, Phys. Rev. B **47**, 2138 (1993).
[2] M. A. Grishin *et al.*, Appl. Phys. A: Mater. Sci. Process. **76**, 299 (2003).
[3] J. M. Nicholls, P. Martensson, and G. V. Hansson, Phys. Rev. Lett. **54**, 2363 (1985).
[4] P. Martensson, A. Cricenti, and G. V. Hansson, Phys. Rev. B **32**, 6959 (1985).
[5] E. Landemark, C. J. Karlsson, Y.-C. Chao, and R. I. G. Uhrberg, Phys. Rev. Lett. **69**, 1588 (1992).
[6] L. S. O. Johansson, E. Landemark, C. J. Karlsson, and R. I. G. Uhrberg, Phys. Rev. Lett. **63**, 2092 (1989); L. S. O. Johansson, E. Landemark, C. J. Karlsson, and R. I. G. Uhrberg, *ibid.* **69**, 2451 (1992).
[7] Y. G. Ding, C. T. Chan, and K. M. Ho, Phys. Rev. Lett. **67**, 1454 (1991); Y. G. Ding, C. T. Chan, and K. M. Ho, *ibid.* **69**, 2452 (1992).
[8] S. Hasegawa and S. Ino, Phys. Rev. Lett. **68**, 1192 (1992).
[9] Y. Nakajima, S. Takeda, T. Nagao, S. Hasegawa, and X. Tong, Phys. Rev. B **56**, 6782 (1997).
[10] J. Viernow, M. Henzler, W. L. O'Brien, F. K. Men, F. M. Leibsle, D. Y. Petrovykh, J. L. Lin, and F. J. Himpsel, Phys. Rev. B **57**, 2321 (1998).
[11] X. Tong, C. S. Jiang, and S. Hasegawa, Phys. Rev. B **57**, 9015 (1998).
[12] S. Hasegawa *et al.*, Prog. Surf. Sci. **60**, 89 (1999).
[13] X. Tong, S. Ohuchi, N. Sato, T. Tanikawa, T. Nagao, I. Matsuda, Y. Aoyagi, and S. Hasegawa, Phys. Rev. B **64**, 205316 (2001).
[14] T. Nagao, T. Hildebrandt, M. Henzler, and S. Hasegawa, Phys. Rev. Lett. **86**, 5747 (2001).
[15] H. M. Zhang, K. Sakamoto, and R. I. G. Uhrberg, Phys. Rev. B **64**, 245421 (2001).
[16] R. I. G. Uhrberg, H. M. Zhang, T. Balasubramanian, E. Landemark, and H. W. Yeom, Phys. Rev. B **65**, 081305(R) (2002).
[17] J. N. Crain, K. N. Altmann, C. Bromberger, and F. J. Himpsel, Phys. Rev. B **66**, 205302 (2002).
[18] M. Ueno, I. Matsuda, C. Liu, and S. Hasegawa, Jpn. J. Appl. Phys., Part 1 **42**, 4894 (2003).
[19] T. Hirahara *et al.*, Surf. Sci. **569**, 191 (2004).
[20] J. N. Crain, J. L. McChesney, F. Zheng, M. C. Gallagher, P. C. Snijders, M. Bissen, C. Gundelach, S. C. Erwin, and F. J. Himpsel, Phys. Rev. B **69**, 125401 (2004).
[21] S. C. Erwin, Phys. Rev. Lett. **91**, 206101 (2003).
[22] J. L. McChesney, J. N. Crain, V. Perez-Dieste, F. Zheng, M. C. Gallagher, M. Bissen, C. Gundelach, and F. J. Himpsel, Phys. Rev. B **70**, 195430 (2004).
[23] H. Aizawa and M. Tsukada, Phys. Rev. B **59**, 10923 (1999).
[24] K. B. Blagoev and K. S. Bedell, Phys. Rev. Lett. **79**, 1106 (1997).
[25] R. Losio, K. N. Altmann, and F. J. Himpsel, Phys. Rev. B **61**, 10845 (2000).
[26] K. N. Altmann, N. Gilman, J. Hayoz, R. F. Willis, and F. J. Himpsel, Phys. Rev. Lett. **87**, 137201 (2001).
[27] R. P. Madden, D. L. Ederer, and K. Codling, Phys. Rev. **177**, 136 (1969).
[28] E. W. Plummer *et al.* (unpublished).